DYNAMICS OF ELECTRODIFFUSION FRICTION PROBES. II. SHAPE-DEPENDENT IMPEDANCE

Ondrej WEIN[1], Vaclav SOBOLIK[2] and Jaroslav TIHON[3]

Institute of Chemical Process Fundamentals, Academy of Sciences of the Czech Republic, 165 02 Prague 6-Suchdol, Czech Republic; e-mail: [1] webox@icpf.cas.cz, [2] vs@icpf.cas.cz, [3] tihon@icpf.cas.cz

Received October 18, 1996
Accepted December 19, 1996

The existing linear (impedance) theory of frequency response is corrected and generalized for electrodiffusion friction probes of any shape. Special attention is paid to the dynamic calibration of real electrodiffusion probes with uncertain geometry by the potentiostatic (voltage-step) transient method.
Key words: Unsteady diffusion layer; Turbulence measurements; Frequency response.

In most cases[1–5], the electrodiffusion (ED) technique is used in hydrodynamic measurements under unsteady flow conditions. For this reason, the dynamic behaviour of electrodiffusion friction probes (EDFP) is of primary interest and it has been studied intensively from the dawn of limiting diffusion current methods[1,2]. State of the art in the field of linear (small-amplitude) dynamics of EDFP is given in ref.[5] almost completely with an exception of the use of similarity approximation to ED impedance[3] in the analysis of the wavy film flow[6].

The main purpose of the present paper is to correct the existing theory[5] of frequency response of EDFP in pulsating shear flows and to generalize it for a convex working electrode of any shape. The common approach[1,2,5] tacitly assumes that all the fundamental parameters of dynamic theory (geometry of the electrode, concentration and diffusivity of the depolarizer) are known with an acceptable accuracy. However, we interpret the same theory in terms of two parameters of a single dynamic calibration experiment – the potentiostatic transient[3,6,7] – which was analysed in our previous paper[8]. New theoretical results about the response of EDFP of arbitrary convex shape to the harmonical superposed shear flow fluctuations are presented in the form of empirical formulas suitable for the computer-aided diagnostics of flow.

THEORETICAL

Formulation and Linearization of Transport Equations

When neglecting the side effects (ohmic and charge-transfer resistances, migration, *etc.*) commonly encountered in any ED experiment[7,8], the theory of ED transport pro-

cesses can be simplified to unsteady convective diffusion of a single component (a depolarizer in electrodiffusion applications) between streaming solution and a reactive surface (working electrode) under one-dimensional flow kinematics. The approximation of concentration boundary layer (high Peclet number) used in the present analysis means that:

1. Both the longitudinal and transversal diffusions are neglected.

2. Existence of a region of constant composition, $c = c^{\mathrm{b}}$, outside the diffusion layer, $z >> \delta(x)$, is postulated.

3. Velocity field within the diffusion layer of a small ED probe is described in the linear approximation

$$v_x = q(t)\, z,\ v_z = v_y = 0. \tag{1}$$

Under these assumptions, the elliptic equation, $\dot{c} = D\nabla^2 c$, simplifies to the parabolic form

$$\partial_t c + q(t)\, z\, \partial_x c = D\, \partial^2_{zz} c \tag{2}$$

with the boundary conditions which express:

1. limiting diffusion currents regime at the electrode surface,

$$c|_{z=0} = 0\ , \quad \text{for } (x, y) \in A\ , \tag{3a}$$

2. presence of fresh solution far from the diffusion layer,

$$c|_{z=\infty} = c^{\mathrm{b}}\ , \tag{3b}$$

3. inactivity of the surface neighbouring on the electrode,

$$\partial_z c|_{z=0} = 0\ , \quad \text{for } (x, y) \notin A\ . \tag{3c}$$

It can be shown for the given parabolic problem that condition (*3c*) can be replaced by the assumption of undisturbed bulk solution just before the forward edge of the electrode. As shown in detail in Part I of this series[8], the coordinate x is locally shifted in

such a way that $x = 0$ corresponds to the forward edge of EDFP at any streamline crossing the electrode surface, so that this assumption can simply be expressed as

$$c|_{z=0} = c^{\mathrm{b}} , \quad \text{for } x < 0 \ . \tag{3d}$$

The ultimate aim is to determine the electric current I corresponding to the total diffusion flux of a depolarizer to the electrode surface A at a given stoichiometry of the electrode reaction. To this end, the surface distribution of the local flux densities must be determined. By an appropriate shift of the longitudinal coordinate x, the local current densities become independent of the transversal coordinate y:

$$i(x,t) = n\boldsymbol{F}D\, \partial_z c(x,z,t)|_{z=0} \ . \tag{4}$$

Therefore, the transversal coordinate y is merely a parameter which need not be considered explicitly when solving the problem of the local current densities.

When studying the effect of small-amplitude periodic flow disturbances, $\varepsilon \to 0$, in linear approximation, it is sufficient to consider harmonic courses of the related fluctuations,

$$q(t) = \bar{q} + \tilde{q} \exp(\mathrm{i}\omega t) = \bar{q}\,(1 + \varepsilon \exp(\mathrm{i}\omega t)) \tag{5}$$

$$c(x,z,t) = \bar{c}(x,z) + \tilde{c}(x,z) \exp(\mathrm{i}\omega t) \tag{6a}$$

$$i(x,t) = \bar{i}(x) + \tilde{i}(x) \exp(\mathrm{i}\omega t) =$$

$$= n\boldsymbol{F}D\, \partial_z(\bar{c}(x,z) + \tilde{c}(x,z) \exp(\mathrm{i}\omega t))|_{z=0} \ . \tag{6b}$$

By substituting the representations (*5*), (*6a*) into Eq. (*2*) and neglecting the terms of the order of ε^2 and higher, we obtain two parabolic boundary-value problems for the steady (time-averaged) and fluctuating parts of the concentration field.

The well-known analytical solution to the *steady part* of the problem,

$$-\bar{q}z\, \partial_x \bar{c} + D\, \partial^2_{zz} \bar{c} = 0 \tag{7}$$

$$\bar{c}\,|_{z=0} = 0 \ , \quad \bar{c}\,|_{z=\infty} = c^{\mathrm{b}} \ , \tag{8a,b}$$

provides explicit formulas for the concentration field and local flux density,

$$\bar{c}/c^{\mathrm{b}} = E(\eta)/E(\infty) \tag{9}$$

$$\bar{i}(x) = \alpha^{1/2} n\boldsymbol{F} D c^{\mathrm{b}}/\sigma(x) \ . \tag{10}$$

All symbols are specified in Symbols and Definitions.

The boundary-value problem for the *complex amplitude* $\tilde{c}(x,z)$ of concentration fluctuations,

$$-\mathrm{i}\omega\tilde{c} - \bar{q}z\,\partial_x\tilde{c} + D\,\partial_{zz}\tilde{c} = \tilde{q}z\,\partial_x\bar{c} \tag{11}$$

$$\tilde{c}|_{z=0} = 0 \ , \qquad \tilde{c}|_{z=\infty} = 0 \ , \tag{12a,b}$$

can be transformed by using the similarity arguments η, ξ,

$$\tilde{c}/c^{\mathrm{b}} = \tfrac{1}{3}\varepsilon f(\eta,\xi)\, E'(\eta)/E(\infty) \ , \tag{13}$$

to the form

$$f'' - 3\eta^2 f' - 6\eta\,\partial_\xi(\xi f) - 9^{2/3}\mathrm{i}\xi f = -9\eta^2 \tag{14}$$

$$f(\eta,\xi) = 0 \ \text{ for } \eta = 0 \ , \ \exp(-\eta^3)\, f(\eta,\xi) \to 0 \ \text{ for } \eta \to \infty \tag{15a,b}$$

with the corresponding representation of the local current densities,

$$\tilde{i}(x) = \tfrac{1}{3}\varepsilon f'(0,\xi)\,\bar{i}(x) \ . \tag{16}$$

Integration of Local Current Densities for Convex Electrodes

Independence of the local current densities on the transversal coordinate y makes it possible to reduce the surface integral in the definition of total current, $I = I(t)$, to quadratures:

$$I(t) = \bar{I} + \tilde{I} \exp(\mathrm{i}\omega t) \ ,$$

where

$$\bar{I} = \iint_A \bar{i}(x)\,\mathrm{d}x\,\mathrm{d}y = \int_0^W \bar{i}_m(l) l\,\mathrm{d}y \ , \quad \tilde{I} = \iint_A \tilde{i}(x)\,\mathrm{d}x\,\mathrm{d}y = \int_0^W \tilde{i}_m(l) l\,\mathrm{d}y \ . \qquad (17a,b)$$

The function $l = l(y)$ characterizes the electrode shape by the distribution of local lengths of thin strip segments, as shown in Fig. 2 of the previous paper[8], and $\bar{i}_m$, $\tilde{i}_m$ stand for the corresponding longitudinal averages along a strip of local length $l = l(y)$ and differential width dy,

$$\bar{i}_m(l) = l^{-1}\int_0^l \bar{i}(x)\,\mathrm{d}x \ , \quad \tilde{i}_m(l) = l^{-1}\int_0^l \tilde{i}(x)\,\mathrm{d}x \ . \qquad (18a,b)$$

With the obvious proportionalities, $\bar{i}_m(x)/\bar{i}_m(a) = (x/a)^{-1/3}$, $\xi(x)/\xi(a) = (x/a)^{2/3}$, and the alternative expression for the area, $S_A = \int_0^W l\,\mathrm{d}y$, these expressions can be further simplified:

$$\bar{I}/S_A = (\tfrac{9}{4}\alpha)^{1/2} n\boldsymbol{F} c^{\mathrm{b}} D^{2/3} (\bar{q}/L_{\mathrm{e}})^{1/3} \qquad (19)$$

and

$$\tilde{I}/\bar{I} = \tfrac{1}{3}\varepsilon \int_0^W G[\xi(l)] l^{2/3}\,\mathrm{d}y / \int_0^W l^{2/3}\,\mathrm{d}y \ , \qquad (20a)$$

where

$$L_{\mathrm{e}} = \left(\int_0^W l\,\mathrm{d}y / \int_0^W l^{2/3}\,\mathrm{d}y \right)^3 \qquad (21)$$

$$G[\xi] = \xi^{-1} \int_0^\xi f'(0,s)\,\mathrm{d}s \ . \qquad (22)$$

In laboratory practice, the ED probes are calibrated under transport conditions (overvoltage, solution composition, current densities level) which are analogous to those applied in the related hydrodynamic experiments. Commonly, the dynamic calibration consists of determining the steady current $\bar{I}$ under a given flow speed and the speed-independent Cottrell coefficient,

$$k_C/S_A = \pi^{-1/2} n\boldsymbol{F} c^{\mathrm{b}} D^{1/2} \ , \qquad (23)$$

from the early stage, $I(t) \approx k_C t^{-1/2}$, $t \to 0$, of the voltage-step (potentiostatic) transient[3,6–8]. The combination of these two calibration parameters provides the potentiostatic transient time, $t_0 = (k_C/\bar{I})^2$. It is suitable to use this experimentally available time scale for normalizing the frequency of fluctuations according to Eqs (*19*), (*23*):

$$\Omega \equiv \omega t_0 = \omega(\bar{I}/k_C)^2 = \beta\xi(L_e) = \beta\psi^{-1}\xi(L) \ , \qquad (24)$$

where the equivalent transport length L_e is defined by Eq. (*21*) and $\psi = (L/L_e)^{2/3}$. By using this new dimensionless frequency Ω, Eq. (*20a*) can be rearranged in the form

$$\tilde{I}/\bar{I} = \tfrac{1}{3}\varepsilon H_A(\Omega) \ , \qquad (25)$$

where

$$H_A(\Omega) = \int_0^W G[(l/L_e)^{2/3}\beta^{-1}\Omega] l^{2/3} \, dy / \int_0^W l^{2/3} \, dy \ , \qquad (20b)$$

is the renormalized electrodiffusion impedance, $H_A(0) = 1$. For an infinite strip of constant length, $l(y) = L = L_e$, this expression simplifies to

$$H(\Omega) \equiv G[\beta^{-1}\Omega] \qquad (26)$$

and the general functional for an electrode with arbitrary convex surface A can be written as

$$H_A(\Omega) = \int_0^W H[(l/L_e)^{2/3}\Omega] l^{2/3} \, dy / \int_0^W l^{2/3} \, dy \ . \qquad (20c)$$

Solution for Local Flux Densities

The two-dimensional boundary-value parabolic problem (*14*), (*15a,b*) for determining $f'(0,\xi)$ has an obvious initial solution for $\xi = 0$,

$$f_0(\eta) \equiv f(\eta,0) = \eta \ , \qquad (27)$$

which corresponds to the quasi-steady asymptote of the dynamic response, $f'(0,0) = 1$. With this initial profile, the problem can be solved numerically by the finite-difference method[1,2] or by using series representations and integrating a consecutive set of ordinary differential equations[5].

Series Representation for Low Frequencies

Assuming a solution in the form of the power series,

$$f(\eta,\xi) = \sum (i\xi/9^{1/3})^m f_m(\eta) \qquad (28)$$

$$f'(0,\xi) = \sum (i\xi/9^{1/3})^m f_m'(0) \ , \qquad (29)$$

for $m = 0, 1, \ldots$, we obtain a consecutive set of linear ordinary real-valued differential equations with homogeneous boundary conditions:

$$f_m'' - 3\eta^2 f_m' - 6\eta(m+1) f_m = 9 f_{m-1} \qquad (30)$$

$$f_m(0) = 0 \quad \text{and} \quad \lim_{\eta\to\infty}[\exp(-\eta^3) f_m(\eta)] = 0 \ . \qquad (31a,b)$$

We solved this problem using the Runge–Kutta integration with iterative adjusting of the set of initial values of $f_m'(0)$ which constitutes the goal of the calculation. The asymptotic behaviour of the functions f_m is of algebraic nature, $f_m(\eta) \approx k_m \eta^{\lambda(m)}$, in accordance with the boundary condition (*31b*). The coefficients k_m are extremely sensitive to the initial conditions and change signs when the estimates of $f_m'(0)$ oscillate closely around the correct values. This behaviour was used in an automated iteration with halving the interval between the upper and lower estimates. The accuracy of the results given in Table I depends merely on the accuracy of the Runge–Kutta integration. We estimate the accuracy of the reported values of $f_m'(0)$ to 15 ÷ 18 (for $0 \le m < 25$), 12 ÷ 15 (for $25 < m \le 60$), and 8 ÷ 12 (for $60 < m \le 80$) valid decimal digits. The function $f'(0,\xi)$ and the corresponding coefficients $f_m'(0)$ are simply related to $h'(0,\xi)$ and $h_m'(0)$ in ref.[5]:

$$f'(0,\xi)/h'(0,\xi) = 1/h_0'(0) = 3^{5/3}\Gamma(\tfrac{4}{3}) = 5.572416712... \qquad (32a)$$

TABLE I
Coefficients of the low-frequency expansion in Eqs (*29*), (*32a,b*), and (*38*)

m	$f_m'(0)$	$h_m'(0)$	*m*	$f_m'(0)$	$h_m'(0)$
0	1.00000000000000E+00	1.79455E–01	30	3.38963527500462E–20	1.74455E–30
1	–1.14974094664877E+00	–9.91918E–02	31	–4.02578734822197E–21	–9.96096E–32
2	8.54159839686774E–01	3.54270E–02	32	4.68041044495344E–22	5.56741E–33
3	–4.89124867078785E–01	–9.75290E–03	33	–5.33015164820388E–23	–3.04809E–34
4	2.31840091629698E–01	2.22240E–03	34	5.94959900852007E–24	1.63567E–35
5	–9.46771769768061E–02	–4.36312E–04	35	–6.51302216874309E–25	–8.60815E–37
6	3.41912608731558E–02	7.57507E–05	36	6.99622788522909E–26	4.44539E–38
7	–1.11224651655421E–02	–1.18465E–05	37	–7.37833618492431E–27	–2.25384E–39
8	3.30419903435304E–03	1.69190E–06	38	7.64329180198797E–28	1.12244E–40
9	–9.05988700729548E–04	–2.23024E–07	39	–7.78095934048320E–29	–5.49335E–42
10	2.31227739180442E–04	2.73645E–08	40	7.78770334324449E–30	2.64321E–43
11	–5.53097966347605E–05	–3.14680E–09	41	–7.66641742717581E–31	–1.25093E–44
12	1.24704202663288E–05	3.41089E–10	42	7.42603018689681E–32	5.82530E–46
13	–2.66290620916180E–06	–3.50156E–11	43	–7.08057072717885E–33	–2.67023E–47
14	5.40751321925595E–07	3.41840E–12	44	6.64791668786955E–34	1.20527E–48
15	–1.04793035528410E–07	–3.18476E–13	45	–6.14836860349893E–35	–5.35894E–50
16	1.94396512374337E–08	2.84022E–14	46	5.60319638960292E–36	2.34787E–51
17	–3.46123911271785E–09	–2.43116E–15	47	–5.03328767798436E–37	–1.01393E–52
18	5.92916083862658E–10	2.00214E–16	48	4.45800044331165E–38	4.31734E–54
19	–9.79246784548293E–11	–1.58969E–17	49	–3.89428651233348E–39	–1.81311E–55
20	1.56225512229404E–11	1.21925E–18	50	3.35611604730519E–40	7.51193E–57
21	–2.41165417953410E–12	–9.04844E–20	51	–2.85419934170942E–41	–3.07127E–58
22	3.60789578916636E–13	6.50777E–21	52	2.39597520589209E–42	1.23947E–59
23	–5.23818720978210E–14	–4.54232E–22	53	–1.98581662549150E–43	–4.93868E–61
24	7.39019154210756E–15	3.08086E–23	54	1.62539465936028E–44	1.94335E–62
25	–1.01435847364383E–15	–2.03295E–24	55	–1.31413989565272E–45	–7.55357E–64
26	1.35600440409952E–16	1.30652E–25	56	1.04974557311182E–46	2.90077E–65
27	–1.76726379786610E–17	–8.18607E–27	57	–8.28665663001798E–48	–1.10085E–66
28	2.24758965452548E–18	5.00507E–28	58	6.46572725738043E–49	4.12938E–68
29	–2.79179870216956E–19	–2.98880E–29	59	–4.98752381647689E–50	–1.53134E–69

$$h_m'(0) = h_0'(0)\, 9^{-m/3} f_m'(0) \quad . \tag{32b}$$

The values of $h_m'(0)$ given in ref.[5] are correct up to 5–6 digits, except for two misprints which should be corrected as follows: $h_4'(0) = 0.222249\text{E}{-2}$ and $h_{12}'(0) = 0.341089\text{E}{-9}$.

With an accuracy to 8 valid digits, the known sequence $f_m'(0)$ for $25 < m < 80$ fulfils the following recurrence rule:

$$-f_{m-1}'(0)/f_m'(0) = 0.85780674\, M_m^{1/3} + 0.1905811\, M_m^{-2/3} \quad , \tag{33}$$

where $M_m = [(m + 0.5)(m - 1)]$. The same accuracy of $f_m'(0)$ is guaranteed when the rule (*33*) is used recursively up to $m = 80$, starting with the known value of $f_m'(0)$ for $m = 25$. We are sure that this result can be used for extrapolation which provides $f_m'(0)$ with an accuracy to about 8 valid digits for any $m > 80$, *i.e.* the inaccuracies do not accumulate. We will show by matching the low- and high-frequency expansions that such an accuracy of $f_m'(0)$ is sufficient to represent $f'(0,\xi)$ up to $\xi = 16$ with an accuracy to about 4 valid digits.

Asymptotic Expansion for High Frequencies

It follows from the recurrence rule (*33*) that the power series (*29*) is convergent for any finite value of ξ. However, the convergence is very slow and a reasonable calculation for $\xi > 15$ requires the coefficients $f_m'(0)$ to be known for m up to 150 with an accuracy to 25 valid digits. This is rather impractical if an asymptotic expansion for high ξ is at hand.

Substituting the expansion

$$f(\eta,\xi) \approx \sum (9^{2/3}\mathrm{i}\xi)^{-(4+3m)/2} F_m(w) \,, \quad w = (9^{2/3}\mathrm{i}\xi)^{1/2}\eta \tag{34a,b}$$

for $m = 0, 1,...$, into Eq. (*14*), we obtain a set of linear differential equations

$$F_0'' - F_0 = -9w^2 \,, \quad F_m'' - F_m = 6w^2 F_{m-1}' - 3(3m - 1)wF_{m-1} \tag{35}$$

with the same homogeneous boundary conditions as in Eqs (*31a,b*). The solution for any m can be expressed by polynomial and exponential functions. In particular:

$$F_0(w) = 9[w^2 + 2 - 2e^{-w}] , \quad F_1(w) = -18[3w^3 + 12w + e^{-w}(w^3 + 3w^2 + 3w)] , \ldots . \quad (36)$$

The corresponding values of $9^{-(1+m)}F_m'(0)$ for calculating the asymptotic representation

$$f'(0,\xi) = \sum (i\xi)^{-(3+3m)/2} 9^{-(1+m)} F_m'(0) , \quad (37)$$

$m = 0, 1, ...$, are given in Table II.

The results of matching the low- and high-frequency representations of $f'(0,\xi)$ are shown in Fig. 1 in the polar representation of $f'(0,\xi)$. Obviously, an acceptable matching (agreement within 1 ÷ 2% of actual values of amplitude and phase shift) is only achieved for $\xi > 15$.

Impedance G[ξ] for Infinite Strip: Matching Low- and High-Frequency Representations

The complex-valued function $G = G[\xi]$ is calculated by integration according to definition (*22*). We assume that the function $f'(0,\xi)$ can be calculated with an acceptable accuracy from the series (*29*) for $\xi < \kappa$ and from the asymptotic expansion (*37*) for $\xi \geq \kappa$. The corresponding representation of G for $\xi \leq \kappa$ is obvious:

$$G[\xi] = \sum (i\xi/9^{1/3})^m f_m'(0)/(m+1) , \quad m = 0, 1, \ldots . \quad (38)$$

TABLE II
Coefficients of the high-frequency asymptotic expansion, Eq. (*37*)

m	$9^{-(1+m)}F_m'(0)$
0	2.000000
1	–3.333333
2	–0.972222
3	–4.861111
4	–48.492959
5	793.441358
6	–19 183.548874

TABLE III

Test of the overlap of the low- and high-frequency representations. *NH* gives the number of terms in the high-frequency part of sum in Eq. (*40*) with an optimized accuracy of the asymptotic expansion

κ	*NH*	Re{*B*(κ)}	Im{*B*(κ)}
6	3	–0.0217	–3.7634
7	4	–0.0329	–3.7182
8	4	–0.0124	–3.6983
9	5	0.0046	–3.7028
10	5	0.0080	–3.7130
11	5	0.0039	–3.7183
12	6	–0.0001	–3.7182
13	6	–0.0016	–3.7162
14	6	–0.0013	–3.7147
15	7	–0.0005	–3.7142
16	7	–0.0001	–3.7140
17	7	–0.0325	–3.6949
Ref.[5]	–	0	–3.715

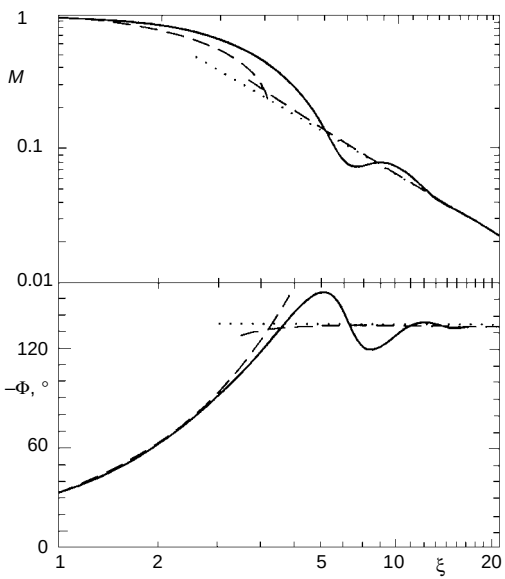

FIG. 1

Normalized local impedances in the polar representation, $M = |f'(0,\xi)|$, $\Phi = \arg(f'(0,\xi))$. Solid lines: exact result; dotted lines: single-term asymptotic expansion, $-\Phi \approx 135°$, $M \approx 2/\xi^{3/2}$; dashed lines for $\xi \to 0$: $-\Phi \approx 31.6° \xi$, $M \approx 1 - 0.04465\ \xi^2$; dashed lines for $\xi \to \infty$: 6-term asymptotic expansion, Eq. (*37*)

When calculating $G = G[\xi]$ for $\xi \geq \kappa$, the integral in (*22*) must be split into two parts,

$$G[\xi] \equiv \xi^{-1}\left[\int_0^{\kappa} + \int_{\kappa}^{\xi} f'(0,s)\,\mathrm{d}s\right] = \xi^{-1}B(\kappa) - \sum (\mathrm{i}\xi)^{-(3+m)/2}\, 9^{-(1+m)} F_m'(0)\, 2/(3m+1)\,, \quad (39)$$

where

$$B(\kappa) = \kappa\sum (\mathrm{i}\kappa 9^{1/3})^m\, f_m'(0)/(m+1) + \kappa\sum (\mathrm{i}\kappa)^{-(3+m)/2}\, 9^{-(1+m)} F_m'(0)\, 2/(3m+1) \quad (40)$$

should be independent of the argument κ over an interval of κ where both the low- and high-frequency expansions overlap, *i.e.* they give the same values of $f'(0,\kappa)$ with an acceptable accuracy. It is obvious from Fig. 1 that the authors[5] are rather optimistic in their claim about a fairly good overlap of low- and high-frequency representations over the interval $6 < \xi < 13$. Actually, the exact values of the impedance oscillate, with a slowly diminishing amplitude, around their asymptotic estimates. This is also documented in Table III giving the values of the "constant" $B(\kappa)$, which still oscillates in the interval $6 < \xi < 13$.

An acceptable overlap cannot be achieved until $\kappa > 15$. Using the numerical results about $B = \mathrm{B}(\kappa)$ for $\kappa = 16$, we found the matching of the both representations of $G[\xi]$ with an accuracy to 4 valid digits over the interval $16 < \xi < 18$, where the optimized asymptotic representation contains only two terms. The results are documented in Table IV using the polar representation of the complex-valued function $G[\xi]$, as usual in the relevant literature.

RESULTS

Infinite Strip

For a rectangular probe with sides parallel or perpendicular to the flow direction and with neglected effect of transversal diffusion, the impedance is the same as for an infinite strip of the same length L. This is given just by the fundamental impedance $G = G(\xi(L))$ where $\xi(L) = \omega\sigma^2(L)/D$. Its selected values are given in Table IV. However, more suitable for applications in ED measurements with real, well-calibrated probes of uncertain geometrical parameters A, L, *etc.* is the renormalized representation of impedance characteristics in the form $H = H(\Omega)$, see Eqs (*24*) and (*25*), whose argument can be calculated from easily accessible calibration data on t_0. The function $H = H(\Omega)$ can be obtained by applying the transformation rule (*26*), $H(\Omega) = G[\xi(L)]$, $\Omega = \beta^{-1}\xi(L) = \omega t_0$. The resulting numerical data about $H[\Omega]$ were represented by the following system of empirical formulas

$$\mathrm{Re}\{H[\Omega]\} = \begin{cases} \Sigma_{k=0}^{4} a_{Rk}(\Omega/\Omega_1)^{2k} / \Sigma_{k=0}^{4} b_{Rk}(\Omega/\Omega_1)^{2k} & ;\ \Omega/\Omega_1 < 1 \\ K(\Omega/\Omega_1)^{-3/2} \Sigma_{k=0}^{4} c_{Rk}(\Omega_1/\Omega - 1/r)^k & ;\ 1 < \Omega/\Omega_1 < r \\ K(\Omega/\Omega_1)^{-3/2} & ;\ r < \Omega/\Omega_1 \end{cases} \qquad (41a,b,c)$$

$$-\mathrm{Im}\{H[\Omega]\} = \begin{cases} \Sigma_{k=0}^{4} a_{Ik}(\Omega/\Omega_1)^{2k+1} / \Sigma_{k=0}^{4} b_{Ik}(\Omega/\Omega_1)^{2k} & ;\ \Omega/\Omega_1 < 1 \\ J(\Omega/\Omega_1)^{-1} - K(\Omega/\Omega_1)^{-3/2} \Sigma_{k=0}^{4} c_{Ik}(\Omega_1/\Omega - 1/r)^k & ;\ 1 < \Omega/\Omega_1 < r \\ J(\Omega/\Omega_1)^{-1} - K(\Omega/\Omega_1)^{-3/2} & ;\ r < \Omega/\Omega_1 \end{cases} . \quad (42a,b,c)$$

TABLE IV
Comparison of the new results about $G(\xi)$ with the data from ref.[5]

ξ	Shift, arg(G)				Amplitude, $\lvert G\rvert$			
	low-frequency series		high-frequency expansion		low-frequency series		high-frequency expansion	
	ref.[5]	Eq. (*29*)	ref.[5]	Eq. (*39*)	ref.[5]	Eq. (*29*)	ref.[5]	Eq. (*39*)
0	0.0	0.0			1.0000	1.0000		
1	–15.7	–15.7			0.9729	0.9729		
2	–30.5	–30.5			0.8973	0.8973		
3	–43.7	–43.7			0.7889	0.7889		
4	–54.3	–54.3			0.6688	0.6688		
5	–61.7	–61.7	–62.9	–62.0	0.5570	0.5570	0.5290	0.5397
6	–66.1	–66.1	–65.9	–65.3	0.4670	0.4670	0.4528	0.4610
7	–68.4	–68.4	–68.1	–67.7	0.4019	0.4019	0.3966	0.4031
8	–69.7	–69.7	–69.9	–69.6	0.3561	0.3561	0.3532	0.3585
9	–70.9	–70.9	–71.3	–71.1	0.3221	0.3221	0.3187	0.3231
10	–72.1	–72.1	–72.5	–72.3	0.2943	0.2944	0.2905	0.2942
11	–73.2	–73.3	–73.5	–73.3	0.2705	0.2707	0.2671	0.2702
12	–73.9	–74.2	–74.4	–74.2	0.2497	0.2503	0.2472	0.2499
13	–73.3	–75.0	–75.1	–75.0	0.2313	0.2327	0.2302	0.2326
14		–75.7	–75.8	–75.6		0.2175	0.2154	0.2175
15		–76.2	–76.3	–76.2		0.2043	0.2024	0.2043
16		–76.7		–76.7		0.1927		0.1927

Here, $\Omega_1 = 10\beta = 4.881039...$ and other adjustable parameters are given in Table V. The parameters were adjusted to minimize the relative difference $\Delta = \max\{|\mathrm{Re}\{H_{\mathrm{emp}}\}/\mathrm{Re}\{H_{\mathrm{num}}\} - 1|\}$ or $\Delta = \max\{|\mathrm{Im}\{H_{\mathrm{emp}}\}/\mathrm{Im}\{H_{\mathrm{num}}\} - 1|\}$ between the correct value H_{num} and its estimate H_{emp} from the empirical formulas (*41*), (*42*). The renormalized impedance $H[\Omega]$ is shown in Fig. 2 in the polar representation common in impedance measurements.

Geometric considerations related to the impedance calculations for electrodes of arbitrary shape are analogous to the problem of determining the shape-dependent potentiostatic transients which was dealt with in our previous paper[8]. In the present work, we use the same notation in describing the related geometric transformations and refer to the geometric schemes given there[8].

Circular Electrode

For the circle of radius R and the centre located at the point $[0,R]$, the shape characteristics can be expressed in the form $l(y)/L = (l - (y/R - 1)^2)^{1/2}$, $L = W = 2R$. The substitution $s^{1/2} = l(y)/L = \psi_C^{-3/2}\, l(y)/L_e$ into Eqs (*21*), (*20c*) gives

$$\psi_C = \left[\int_0^1 s^{1/3}(1-s)^{-1/2}\,\mathrm{d}s \Big/ \int_0^1 s^{1/2}(1-s)^{-1/2}\,\mathrm{d}s\right]^2 = 1.1474442... \qquad (43a)$$

$$H_C[\Omega] = \int_0^1 H[\psi_C \Omega s^{1/3}] s^{1/3}(1-s)^{-1/2}\,\mathrm{d}s \Big/ \int_0^1 s^{1/3}(1-s)^{-1/2}\,\mathrm{d}s \ . \qquad (43b)$$

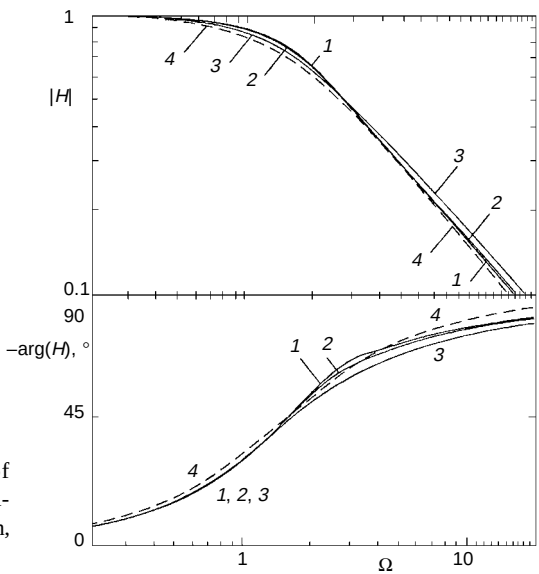

FIG. 2
Renormalized impedances for EDFP of various shape. *1* Strip; *2* circles and ellipses; *3* triangles; *4* similarity approximation, $H_*[\Omega] = (1 + 2/3\mathrm{i}\Omega)^{-1}$

TABLE V
Empirical representation of $H[\Omega]$ for different probes

k	Eq. (*41a*)		Eq. (*42a*)		Eq. (*41b,c*)	Eq. (*42b,c*)
	a_{Rk}	b_{Rk}	a_{Ik}	b_{Ik}	c_{Rk}	c_{Ik}
			$H_S[\Omega]$ for stripe probes			
0	1.0000	1.000	2.7637	1	1	1
1	–1.1104	5.436	–1.7748	4.269	–0.0249	0.0355
2	2.0735	14.464	6.7994	8.934	–0.1268	–0.3738
3	7.6860	7.620	4.4744	10.88	2.0033	1.2465
4	–0.0280	78.100	–0.00304	18.67	–3.5091	–0.6273
r					1.56	1.56
$K = K_S$					0.08944	0.08944
$J = J_S$						0.37072
Δ_{max}		7E–5		3E–5	1E–4	8E–5
			$H_C[\Omega]$ for circular and elliptic probes			
0	1	1	2.7851	1	1	1
1	–1.793	5.0871	–0.04122	5.3453	0	0.02285
2	7.3802	12.557	14.2682	14.8653	–0.05962	–0.02328
3	–0.9742	31.084	4.0796	35.8976	0.21737	0.06327
4	1.075	19.263	0.3083	17.8829	–0.16554	0.04705
r					1.8	1.9
$K = K_C$					0.09687	0.09793
$J = J_C$						0.38457
Δ_{max}		3E–4		4E–4	2E–4	9E–5
			$H_T[\Omega]$ for triangular probes			
0	1	1	2.8426	1	1	1
1	–0.2148	7.368	0.0043	6.5023	–0.08868	0.01727
2	14.100	28.45	20.2759	19.4357	0.00508	0.04004
3	–0.221	87.49	–0.2217	38.5032	–0.01178	–0.00672
4	1.318	10.82	2.8622	22.6856	0.0085	–0.01758
r					4	2.5
$K = K_T$					0.12662	0.1368
$J = J_T$						0.4319
Δ_{max}		2E–4		2E–4	2E–5	8E–5

The integral (*43b*) was calculated with $H[\Omega]$ generated by summing the series (*29*) for $\xi < 16$ and using the two-term expansion (*41c*) and (*42c*) at higher ξ. The singularities of the integral (*43b*) were treated analytically by expanding the integrand into series for $s \to 0$ and $s \to 1$ and integrating the resulting sum term-by-term. The numerical data on $H_C[\Omega]$ were fitted with the analogous system of empirical formulas (*41*), (*42*) with the resulting parameters given in Table V.

Distribution of local transport lengths in the general form $l(y)/L = (1 - a(y - y_0)^2)^{1/2}$ can also be obtained for an ellipse of any orientation to the flow direction and, hence, the normalized impedance characteristic is the same, $H_A[\Omega] = H_C[\Omega]$. The only direction-sensitive parameter of a revolving elliptical probe is the maximum transport length, L_e, ref.[8].

Triangular Electrode

The shape characteristic of a right-angled triangle with the side L parallel to the flow direction and the side w perpendicular is obviously linear, $l(y)/L = y/w$. The substitution $s^{3/5} = l(y)/L = \psi_C^{-3/2}\, l(y)/L_e$ into Eqs (*21*) and (*20c*) gives:

$$\psi_T = \left[\int_0^1 \mathrm{d}s / \int_0^1 s^{1/5}\, \mathrm{d}s \right]^2 = 1.44 \qquad (44a)$$

$$H_T[\Omega] = \int_0^1 H[\psi_T \Omega s^{2/5}]\, \mathrm{d}s \ . \qquad (44b)$$

The result of numerical integration was fitted in the same way as for the circular probes. The parameters of the empirical formulas (*41*) and (*42*) are given in Table V.

By using the analogous reasoning as in ref.[8], it can be shown that the normalized impedance of any triangle is the same. The only direction-sensitive parameter of a revolving triangular probe is the equivalent transport length[8], L_e.

Rectangular Electrode in a Flow of Varying Direction

The calculation of the distribution function $l = l(y)$ for a rectangular electrode of sides L_0, w_0 and angle ϕ is shown in ref.[8]. The slanted rectangle can be taken as a union of two triangular electrodes of width w_T and a single strip electrode of finite width w_S. All the three parts have a common maximum transport length L. With the known impedance characteristics for strips and triangles, the expression for the direction-dependent impedance characteristics for a revolving rectangle follows directly from the general definitions (*21*) and (*20c*):

$$\psi_R = [(w_S + \tfrac{6}{5}w_T)/(w_S + w_T)]^2 \qquad (45a)$$

$$H_R[\Omega] = (w_S H[\psi_R\Omega] + w_T H_T[\psi_R\Omega])/(w_S + \tfrac{6}{5}w_T) \ , \qquad (45b)$$

where w_S, w_T are the lengths of lateral subintervals from (0, W) occupied by the rhomboidal and triangular parts of the rectangular electrode, respectively (see Fig. 7 in ref.[8], where the directional dependence of w_S, w_T, and L_e is discussed in detail).

Series Representation for Low and Medium Frequencies

The impedance characteristic of any convex ED probe can be represented by a convergent series. Substitution of the low-frequency series (*38*) into relations (*20b*) and (*26*), and integration of the resulting sum term-by-term gives

$$H_A[\Omega] = \sum_{m=0}^{\infty} k_{A,m}(\mathrm{i}\Omega)^m = \sum_{m=0}^{\infty} \Lambda_A(m) \left(\frac{\mathrm{i}\Omega}{9^{1/3}\beta} \right)^m \frac{f_m'(0)}{m+1} \ , \qquad (46)$$

where $\Lambda_A(m)$ are the only shape-dependent parameters,

$$\Lambda_A(m) = \int_0^W (l/L_e)^{2(m+1)/3} \, \mathrm{d}y / \int_0^W (l/L_e)^{2/3} \, \mathrm{d}y \ . \qquad (47)$$

In particular, for stripes we have $\Lambda_S(m) = 1$, for triangles $\Lambda_T(m) = (6/5)^{2m}\, 5/(5 + 2m)$, and

$$\Lambda_C(m) = \psi_C^m \frac{\Gamma(\frac{m+4}{3})\, \Gamma(\frac{11}{6})}{\Gamma(\frac{2m+11}{6})\, \Gamma(\frac{4}{3})} \qquad (48)$$

for circles and ellipses. A few first coefficients $k_{A,m}$ are given in Table VI.

Asymptotic Expansion for High Frequencies

If the shape characteristic $l = l(y)$ does not contain a region where $l \to 0$, the asymptotic expansion for $\Omega \to \infty$ according to the result for the strip,

$$H[\Omega] \approx -\mathrm{i}J_S(\Omega/\Omega_1)^{-1} + (1 - \mathrm{i})K_S(\Omega/\Omega_1)^{-3/2} \ , \qquad (49)$$

see Eq. (*39*), can be used for a correct asymptotic representation of $H[\psi\Omega(l/L)^{2/3}]$ for $(l/L)^{2/3}\Omega \to \infty$ in the integral transformation (*20c*) with the obvious result

$$H_A[\Omega] \approx -\mathrm{i}J_A(\Omega/\Omega_1)^{-1} + (1-\mathrm{i})K_A(\Omega/\Omega_1)^{-3/2} \ , \qquad (50a)$$

where $J_A = p_{A,1} J_S$, $K_A = p_{A,2} K_S$, and

$$p_{A,1} = \int_0^W \mathrm{d}y / \int_0^W (l/L_\mathrm{e})^{2/3}\,\mathrm{d}y \qquad (50b)$$

$$p_{A,2} = \int_0^W (l/L_\mathrm{e})^{-1/3}\,\mathrm{d}y / \int_0^W (l/L_\mathrm{e})^{2/3}\,\mathrm{d}y \ . \qquad (50c)$$

In other cases, the uniform convergence of integral (*20c*) for $(l/L) \to 0$, $\Omega \to \infty$ should be checked. For convex probes, with triangular ones as a limiting case, this property can be checked before using formulas like (*50a*), by splitting the integral (*44b*) into two parts, $\int_0^1 = \int_0^\varepsilon + \int_\varepsilon^1$, and neglecting the first part for $\varepsilon \to 0$. The values of J_A, K_A calculated according to Eqs (*50a,b,c*) with the coefficients $p_{A,k}$ for circles or ellipses ($A = C$) and triangles ($A = T$) given in Table VI, correspond well with the values of J_A, K_A obtained by empirical fitting of the numerical data on $H_A[\Omega]$, see Table V.

Non-Convex Electrodes

We demonstrated for a class of convex electrodes that the shape-dependent variations of normalized impedance characteristics can be reflected by introducing a single shape-

TABLE VI
The coefficients $k_{A,m}$ and $p_{A,m}$ according to Eqs (*46*) and (*50a*)

m	$A = S$ (strip)		$A = C$ (circle)		$A = T$ (triangle)	
	$k_{A,m}$	$p_{A,m}$	$k_{A,m}$	$p_{A,m}$	$k_{A,m}$	$p_{A,m}$
0	1.000		1.000		1.000	
1	–0.566	1.000	–0.571	1.036	–0.582	1.157
2	0.276	1.000	0.288	1.083	0.318	1.447
3	–0.467		–0.513		–0.634	

dependent parameter $\psi = \psi_A$. The following example demonstrates that such an approach cannot be applied for non-convex electrodes.

Let us consider a pair of strip segments of different lengths L, λL ($\lambda < 1$) and widths κw, w, shown in Fig. 3. According to the definition $\psi = (L/L_e)^{2/3}$, ψ can be expressed for this geometric configuration as

$$\psi^{1/2} = (\kappa + \lambda^{2/3})/(\kappa + \lambda) \quad . \tag{51}$$

Hence, there is a single-parameter family of geometric configurations with constant ψ for $\lambda \in (0, \psi^{-3/2})$. The normalized impedance characteristics for such a family with $\psi^{1/2} = 6/5$ is shown in Fig. 3 and compared with the course for triangular probes (*i.e.* the convex surface with the same ψ). For the extreme case $\lambda \to \psi^{-3/2}$, $\kappa \to 0$, the transient characteristic is the same as for a single strip because the longer of the rectangles has zero width and hence cannot affect the total current.

Note that this example deals with non-convex surfaces. Probably, there is a one-to-one mapping between the form parameter $\psi = \psi_A$ and the normalized impedance characteristics $H_A[\Omega]$ for convex surfaces, but a formal proof of this assumption was not found. Anyway, this example shows that the normalized impedance characteristics $H_A[\Omega]$ are almost shape-independent in the region $\Omega < 2$, see Fig. 3, for a broad class of surfaces which are neither convex nor contiguous.

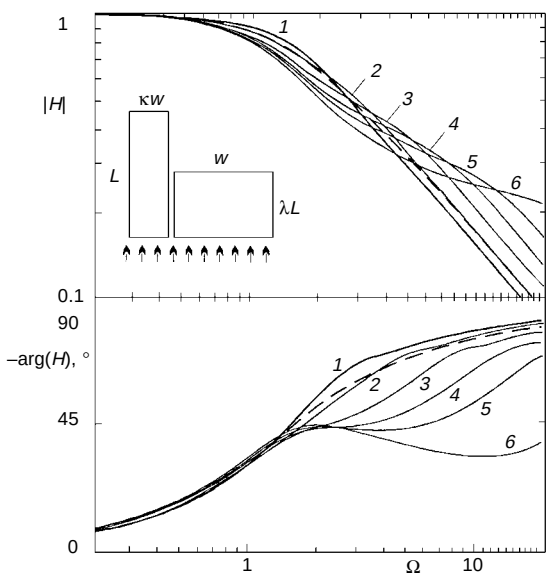

FIG. 3
Renormalized impedances for a parallel combination of two stripes of various length and width with the constant form-parameter $\psi = 36/25$: *1* single strip, $\lambda = \psi^{-3/2}$, $\kappa = 0$; *2* $\lambda = 0.5\psi^{-3/2}$, $\kappa = 0.4$; *3* $\lambda = 0.2\psi^{-3/2}$, $\kappa = 0.5$; *4* $\lambda = 0.1\psi^{-3/2}$, $\kappa = 0.4$ *5* $\lambda = 0.05\psi^{-3/2}$, $\kappa = 0.3$; *6* $\lambda = 0.01\psi^{-3/2}$, $\kappa = 0.1$; dashed lines: the result for a triangle ($\psi_T = 36/25$)

DISCUSSION AND CONCLUSIONS

A new accurate series solution to the title problem is given, see Table I. The improved accuracy (10–15 valid digits) and higher number of terms (80 terms directly and unlimited number of terms from accurate extrapolation sequence, Eq. (*33*)) makes it possible to use the series representation of normalized local current densities $f'(0,\xi)$, up to $\xi = 16$. The asymptotic expansion for $\xi \to \infty$ with unlimited number of terms is given in a simple analytical form. The comparison with the previous calculations[5] shows that the series and asymptotic expansion representations do not match within acceptable accuracy until $\xi > 16$ where two terms of the asymptotic expansion guarantee the accuracy of G to four decimal digits. However, the inaccuracy of the local solution does not appreciably affect the integral solution G. The maximum error of the results given in ref.[5] is 1° in arg ($G[\xi]$) and 1% in $|G[\xi]|$ in the region $12 < \xi < 15$ (Table IV).

The impedance characteristics normalized by the time-averaged current $\bar{I}$ and the corresponding transient time t_0, *i.e.* in the form $H_A[\Omega]$, vary in extremely narrow limits over the set of convex surfaces. In particular, the courses of $H_A[\Omega]$ in the low-frequency region, $\Omega < 2$, are almost the same for any surface. The extreme courses correspond to infinite strips ($\psi = 1$) and triangles ($\psi = 1.44$) as shown in Figs 2 and 3. The courses for strips and circles are so close to one another that it is difficult to distinguish them in Fig. 2. For a rough estimate, the similarity approximation[3,6,8]

$$H_*[\Omega] = 1/(1 + \tfrac{2}{3}\mathrm{i}\Omega) \qquad (52)$$

seems to be quite acceptable. For more accurate calculations, the normalized impedance characteristics of particular convex surfaces – strips, triangles, rectangles, circles, and ellipses – are represented by accurate empirical formulas, see Eqs (*41*), (*42*) and Table V.

The impedance characteristics $H_A[\Omega]$, operationally defined in Eqs (*24*) and (*25*), are normalized by the pair of parameters $\bar{I}$, t_0, easily accessible from the dynamic (voltage-step transient) calibration experiment[7,8]. Their use for correcting the primary ED data on diffusion inertia of EDFP, in particular for an estimate of the cut-off frequency in experimental turbulent spectra, should be requested in every experimental ED study.

SYMBOLS AND DEFINITIONS

(Meaning of symbols marked with *) can become obvious from Fig. 2 in ref.[8])

A	surface of electrode
c	$= c(x,z,t)$, concentration field of depolarizer, mol m^{-3}
c^b	bulk concentration of depolarizer, mol m^{-3}
D	diffusivity of depolarizer, m^2 s^{-1}

$E(\eta)$	$\equiv \int_0^\eta \exp(-s^3)\,\mathrm{d}s$, similarity representation of steady concentration profile
$E(\infty)$	$= \Gamma(\frac{4}{3})$
$\boldsymbol{F}$	= 96484.56 C mol^{-1}, Faraday constant
f	$= f(\eta,\xi)$, complex-valued similarity representation of concentration fluctuations
G	$= G(\xi)$, normalized impedance for strip EDFP, fundamental impedance, Eq. (*22*)
$H[\Omega]$	$= H_S[\Omega]$, renormalized impedance for strip electrode, Eq. (*24*)
$H_A[\Omega]$	shape-dependent normalized impedance for surface A, Eq. (*25*)
i	$= i(x,y,t)$, local current density, A m^{-2}
I	$= I(t)$, total current through EDFP, A
J, J_A	asymptotic parameters in Eqs (*41*), (*42*), (*50*) and Table V
K, K_A	asymptotic parameters in Eqs (*41*), (*42*), (*50*) and Table V
k_C	Cottrell coefficient, Eq. (*23*), A s$^{1/2}$
l	$= l(y)$, local length of strip*), m
L	maximum transport length of electrode*), m
L_e	equivalent transport length of electrode, Eq. (*21*), m
n	number of electrons involved in electrode reaction
q	$= q(t)$, fluctuating wall shear rate, Eq. (*1*), s^{-1}
S_A	area of A, m^2
t	time, s
t_0	$= (k_C/\overline{I})^2$, potentiostatic transient time, s
v_x, v_y, v_z	longitudinal, transversal, and normal velocity component, m s^{-1}
W	transport width of probe*), m
x	locally shifted longitudinal coordinate*), m
y, z	transversal and normal coordinates*), m
α	$= 9^{-2/3}/\Gamma^2(\frac{4}{3})$, constant of Lévêque theory, Eqs (*10*), (*19*)
β	$= (\frac{9}{4}\pi\alpha)^{-1} = 0.48810398...$, constant in definition of transient time, Eq. (*24*)
Δ	$= \Delta(\Omega)$, error of approximation to $H = H(\Omega)$, see text below Eqs (*42*)
Δ_{max}	maximum to Δ, taken over related interval of Ω
$\delta(x)$	$= \frac{2}{3}\alpha^{-1/2}\sigma(x)$, Nernst thickness of diffusion layer for strip, m
ε	$= \tilde{q}/\overline{q}$, normalized complex amplitude of shear rate fluctuations
η	$= 9^{-1/3}z/\sigma(x)$, argument of similarity concentration profiles
ξ	$= \xi(x) = \omega\sigma^2(x)/D$, locally normalized frequency, similarity argument in Eq. (*13*)
ψ	$= \psi_A \equiv (L/L_e)^{2/3} = \left(\int_0^W (l/L)^{2/3}\,\mathrm{d}y / \int_0^W (l/L)\,\mathrm{d}y\right)^2$, form parameter of working electrode
$\sigma(x)$	$= (Dx/\overline{q})^{1/3}$, modified local thickness of diffusion layer, m
ω	frequency of hydrodynamic fluctuations, rad s^{-1}
Ω	$= \omega t_0$, normalized frequency for electrode, Eq. (*24*)

Special symbols

∂_η, ∂_ξ	partial derivative with respect to argument η, ξ, *etc.*
$\overline{q}$	time average of fluctuating quantity $q = q(t)$
$\tilde{q}$	complex amplitude of fluctuating quantity, $q = \overline{q} + \tilde{q}\exp(\mathrm{i}\omega t)$
f', f''	derivatives with respect to η, *e.g.* $f'(0,\xi) = \partial_\eta f(\eta,\xi)\vert_{\eta=0}$

Subscripts

A	arbitrary (commonly: convex and contiguous) plane surface
C	circles and ellipses
R	rectangles
S	infinite stripes
T	triangles
*	similarity approximation

This work was partially supported by the Grant Agency of the Czech Republic under contract No. 104/95/0654 and by the Grant Agency of the Academy of Sciences of the Czech Republic under contract No. A4072502.

REFERENCES

1. Hanratty T. J., Campbell J. A. in: *Fluid Mechanics Measurements* (R. J. Goldstein, Ed.). Hemisphere Publ. Corp., Washington 1983.
2. Nakoryakov V. E., Burdukov A. P., Kashinskii O. N., Geshev P. I.: *Elektrodiffuzionnyi metod issledovaniya lokalnoi struktury turbulentnykh techenii*. Institute of Thermophysics, Novosibirsk 1986.
3. Pokryvaylo N. A., Wein O., Kovalevskaya N. D.: *Elektrodiffuzionnaya diagnostika techenii v suspenziyakh i polimernykh rastvorakh*. Nauka i Tekhnika, Minsk 1988.
4. Grafov B. M., Martemianov S. A., Nekrasov L. N.: *Turbulentnyi diffuzionnyi sloi v elektrokhimicheskikh sistemakh*. Nauka, Moscow 1990.
5. Deslouis C., Gill O., Tribollet B.: J. Fluid Mech. *215*, 85 (1990).
6. Sobolik V., Wein O., Cermak J.: Collect. Czech. Chem. Commun. *52*, 913 (1987).
7. Sobolik V., Tihon J., Wein O., Wichterle K.: J. Appl. Electrochem., in press.
8. Wein O., Sobolik V.: Collect. Czech. Chem. Commun. *62*, 397 (1997).